Magnetocaloric properties of phenolic resin bonded La(Fe,Si)$_{13}$-based plates and its use in a hybrid magnetic refrigerator

Shao-Shan Xu(徐少山)[1,2], Qi Fu(付琪)[3], Yi-Fan Zhou(周益帆)[3], Ling Peng(彭铃)[3], Xin-Qiang Gao(高新强)[1,3,†], Zhen-Xing Li(李振兴)[1], Mao-Qiong Gong(公茂琼)[1], Xue-Qiang Dong(董学强)[1,2], and Jun Shen(沈俊)[1,2,‡]

[1] *Technical Institute of Physics and Chemistry, Chinese Academy of Sciences, Beijing* 100190, *China*
[2] *University of Chinese Academy of Sciences, Beijing* 100049, *China*
[3] *Ganjiang Innovation Academy, Chinese Academy of Sciences, Ganzhou* 341119, *China*

(Received 27 September 2022; revised manuscript received 31 October 2022; accepted manuscript online 3 November 2022)

We present a simple hot press-based method for processing La(Fe,Si)$_{13}$-based compounds consisting of La–Fe–Co–Si–C particles and phenolic resin. The magnetic entropy change ΔS per unit mass for the $LaFe_{10.87}Co_{0.63}Si_{1.5}C_{0.2}$/phenolic resin compounds have nearly the same magnitude with the base materials. With the content of phenolic resin of 5.0 wt%, the compound conductivity is 3.13 $W\cdot m^{-1}\cdot K^{-1}$. In order to measure the cooling performance of La(Fe,Si)$_{13}$-based compounds, the $La(Fe_{11.6-x}Co_x)Si_{1.4}C_{0.15}$ (x =0.60, 0.65, 0.75, 0.80, 0.85)/phenolic resin compounds were pressed into thin plates and tested in a hybrid refrigerator that combines the active magnetic refrigeration effect with the Stirling cycle refrigeration effect. The test results showed that a maximum cooling power of 41 W was achieved over a temperature span of 30 K.

Keywords: magnetocaloric effect, La(Fe, Si)$_{13}$, phenolic resin, magnetic refrigeration, hybrid refrigerator

PACS: 75.30.Sg, 65.40.gd, 75.20.En **DOI:** 10.1088/1674-1056/ac9fbf

1. Introduction

Magnetic refrigeration technology based on magnetocaloric effect (MCE) has been considered as a potential substitute of conventional vapor compression refrigeration due to its intrinsic high-efficiency and environment friendliness.[1–4] The magnetocaloric effect is a magneto-thermodynamic phenomenon that the magnetocaloric materials absorb or emit heat when undergoing a changing magnetic field. It is quantified by the adiabatic temperature change ΔT_{ad} or the isothermal entropy change ΔS.[5] The magnitude is typically a few degrees for ΔT_{ad} when the working field in a practical refrigerator is generated by permanent magnets (maximum 2 T). Using an active magnetic regenerator (AMR) can generate a temperature span exceeding the adiabatic temperature change ΔT_{ad} of the given magnetocaloric material.[6] An AMR is generally a porous bed of magnetocaloric material which simultaneously acts as a refrigerant to generate cooling and a conventional regenerator to exchange heat with the heat transfer fluid and build up a temperature gradient.[6] Most recently, the discovery of room-temperature giant magnetocaloric materials, such as $Gd_5(Si_xGe_{1-x})_4$,[7–9] La(Fe,Si)$_{13}$,[10,11] MnAs-based compounds,[12–14] NiMn-based,[15–17] and $La_{1-x}Ca_xMnO_3$ manganite,[18–20] has pushed the magnetic refrigeration technology a big step forward. Among these magnetocaloric materials, La(Fe,Si)$_{13}$-based compounds are widely accepted as one of the most promising candidates due to their easy and environmentally friendly preparation, low cost, non-toxic constituent elements, and excellent magnetocaloric effect.[21] By partially substituting Fe with Mn[22] or Co,[23] or introducing interstitial hydrogen (H)[24] or carbon (C)[24] in the La(Fe,Si)$_{13}$ crystal structure, the Curie temperature T_c associated with the optimal operating temperature for a magnetocaloric material can be tuned over a large temperature span from $\sim$ 170 K to $\sim$ 340 K, while the large MCE can remain and the hysteresis loss may decrease. The tunable Curie temperature is important for an efficient AMR, as a single material exhibits a large MCE only within a relatively small temperature range near its transition temperature. In order to achieve a high performance refrigerator, multi-layer AMR bed was proposed by arranging different magnetic materials in series along the temperature gradient according to their Curie temperatures.[25]

The large MCE in La(Fe,Si)$_{13}$-based compounds is due to the thermally-induced first-order transition between the ferromagnetic (FM) and paramagnetic (PM) states and the field-induced itinerant–electron metamagnetic (IEM) transition at temperatures near but above T_c.[26]

The performance of the magnetic regenerator is determined not only by the MCE properties, but also by its chemical and mechanical stability, regenerator geometry, and thermal conductivity of the magnetocaloric material.[4] In an efficient AMR cycle, the heat must be timely transferred from the interior of magnetic refrigerant to the heat transfer fluid and hardly

†Corresponding author. E-mail: xqgao@gia.cas.cn
‡Corresponding author. E-mail: jshen@mail.ipc.ac.cn

© 2023 Chinese Physical Society and IOP Publishing Ltd

transported between the magnetocaloric materials in the axial direction.[27] In order to improve the efficiency of heat transfer and reduce the pressure drop, the materials are preferably shaped into regular geometries such as plates other than spheres or flakes with the diameter or plate thickness down to 0.1 mm–0.6 mm.[28] However, it is a challenge to process the brittle La(Fe,Si)$_{13}$-based compounds into plates with small dimensions. Recently, spherical La(Fe,Si)$_{13}$, their hydrides and La(Fe,Co,Si)$_{13}$ were realized by using the rotating electrode process (REP).[29,30] The diameter of these spherical particles can be adjusted within a wide range from 0.1 mm to 1.2 mm. However, this method requires expensive equipment and a big ingot per production cycle. The La(Fe,Co,Si)$_{13}$ plates with thicknesses from 0.25 mm to 1.0 mm and the monolithic regenerator with slots of 0.2 mm were machined by the thermally induced decomposition and recombination (TDR) process.[31] More complex geometries of La(Fe,Co,Si)$_{13}$ magnetic refrigerant blocks, such as the wavy-channel design with a high surface-to-volume ratio and the transverse-fin design without unwanted longitudinal heat-conduction, were successfully prepared through the selective laser melting (SLM) process.[32] However, the SLM blocks generated 29-wt% impurity phases (α-Fe, La-rich and 1:1:1 phase) that would significantly reduce the MCE. There is also a report that the magnetic cooling performance of the porous La(Fe,Si)$_{13}$-based alloys significantly improved by electroless copper plating. After Cu coating, the thermal conductivity as well as corrosion resistance was increased, and the magnetic hysteresis loss was decreased.[33] However, this method required complex electrolyte and accurate control of deposition rate.

Besides thermal performance, a practical magnetic refrigeration device requires good mechanical stability to undergo millions of thermodynamic cycles and periodically varying magnetic field. It has been reported that the bulk La(Fe,Si)$_{13}$ alloy lost its mechanical integrity after the 4th temperature-field cycle and the $\Delta T_{\rm ad}$ simultaneously reduced because of its large volume change during the first-order transition.[34]

For commercial applications, La(Fe,Si)$_{13}$-based materials must be cheaply and mass-fabricated into suitable forms (spheres, plate shapes, wires, *etc*.) for refrigerators without impairing the precious magnetocaloric effect and mechanical stability. However, machining process remains a challenge and key task for practical application since La(Fe,Si)$_{13}$-based intermetallic compounds are very brittle and present a volume change in a changing magnetic field.[35]

Here we present a simple hot press-based method for processing La(Fe,Si)$_{13}$-based compounds. Magnetocaloric effect, thermal properties, and cooling performance are studied experimentally for these La(Fe,Si)$_{13}$-based/phenolic resin plates. The cooling performance was demonstrated in a hybrid refrigerator that combines the active magnetic refrigeration effect with the Stirling cycle refrigeration effect.

2. Hot press method for plate manufacturing

A one-step fabrication strategy is carried out by hot pressing compounds of La(Fe,Si)$_{13}$-based alloy powders and solid phenolic resin (PR) binder (consisting of phenolic resin powder and hexamethylenetetramine powder) at a relatively low temperature. The hot pressing procedure is shown in Fig. 1. The magnetic particles are in contact with each other under applied pressure. Concurrently, PR is rapidly cured by heating and then glues the entire magnetocaloric material powders together into various forms of plate, arc, washer or cylinder shapes corresponding to the molds. If required, secondary processing such as drilling and incising can be easily performed.

Aiming at the quality factor of mechanical strength in the process, the optimum curing condition is determined by the non-isothermal and isothermal differential scanning calorimetry (DSC) analysis of PR.

The non-isothermal DSC curves of PR with the heating rates of 5, 10, 15, and 20 °C·min^{-1} are displayed in Fig. 2(a). Increasing the heating rate resulted in the DSC curves shifting to higher temperature ranges with increased peak width, suggesting that PR can be cured in a reduced time as the heating rate enhances. The peak temperature ($T_{\rm p}$ calculated from the non-isothermal DSC curves) *versus* the heating rate is plotted in Fig. 2(b), wherein a good linear relation can be achieved. By extrapolation of heating rate to zero, the intercept of the straight line can be regarded as the optimal curing temperature ($T_{\rm p}^0$), which is 144.25 °C. We then select integer 150 °C as the molding temperature. Figure 2(c) shows the isothermal DSC curves of PR with a cure temperature of 150 °C. It is noted that the cure reaction displayed a typical autocatalytic characteristic, since the maximum exothermic peak appeared at time > 0. Shown in Fig. 2(d), the experimental isothermal reaction conversion α as a function of time can be obtained from the ratio of integral area of the reaction exothermic peak to the total reaction exotherm, which is calculated from Fig. 2(c) and calculated using

$$\alpha = \frac{1}{\Delta H_0}\int_0^t \frac{{\rm d}H}{{\rm d}t}\,{\rm d}t, \tag{1}$$

where H, t, and ΔH_0 represent the DSC heat flow, the reaction time, and total reaction exotherm. We can find that the conversion α reached up to 98.8% when the PR was heated for 10 min. That is, almost all of the PR powders have bonded together in 10 min. Therefore, the curing condition is selected at 150 °C for 10 min based on a compromise between processing time and conversion. After setting the curing condition, plate-shaped LaFe$_{10.87}$Co$_{0.63}$Si$_{1.5}$C$_{0.2}$/PR (denoted as LFCSC/PR) compounds have been prepared and investigated. The compounds with 2.5-wt% and 5-wt% PRs are denoted as 97.5-LFCSC and 95-LFCSC, respectively.

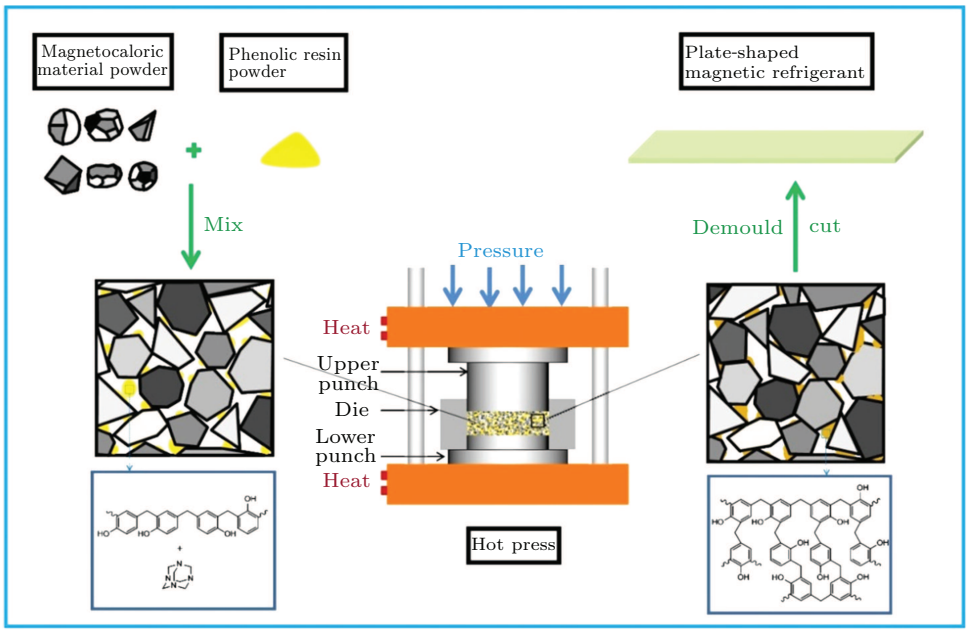


Fig. 1. Photograph of fabrication procedure for plate-shaped $La(Fe,Si)_{13}$/PR compounds.

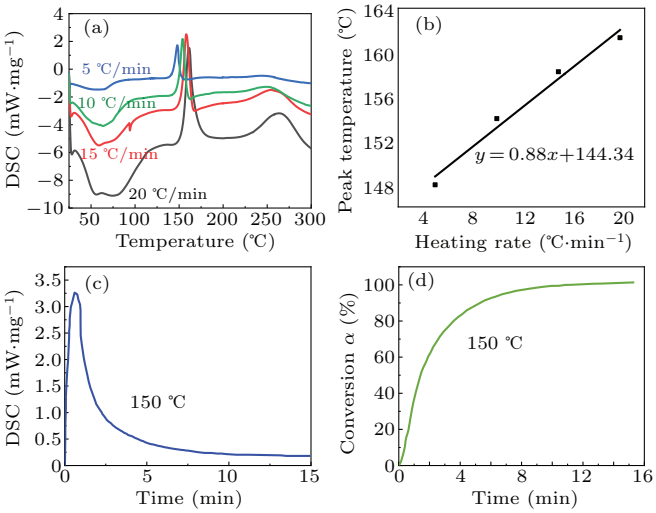


Fig. 2. (a) DSC curves of PR with different heating rates. (b) Relationship between curing temperatures and heating rates of PR. (c) DSC curves of isothermal cure of PR at 150 °C. (d) Experimental isothermal reaction conversion as a function of time of PR.

3. Measurement of the plate properties

3.1. Instrumentation

The crystalline structures were identified by room-temperature powder x-ray diffraction (XRD) with Cu $K\alpha$ radiation. The surface morphologies and the phase composition were analyzed by a S-4300 scanning electron microscopy (SEM) equipped with energy dispersive spectrometer (EDS). The density of bonded samples was measured by the Archimedean method. The measurements of thermal diffusivity were performed with the NETZSCH LFA 427 device. The measurements were performed at the temperature 304 K (at zero magnetic field). The specific heat was measured using a heat capacity option on Quantum Design physical property measurement system (PPMS), and the thermal conductivity κ was calculated using

$$k = \dot{\alpha} \cdot \rho \cdot c_{\mathrm{p}}, \tag{2}$$

where $\dot{\alpha}$, κ, ρ, and c_{p} represent thermal diffusivity, thermal conductivity, density, and specific heat, respectively. The Curie temperature, T_{C}, was determined by the minimum of $\mathrm{d}M/\mathrm{d}T$ of temperature dependence of magnetization $M(T)$, measured in a low magnetic field (0.01 T). The isothermal entropy change, ΔS, was calculated from magnetization isothermal $M(H)$ using the Maxwell relation. Two PT100-type platinum resistance thermometers were used to measure the hot- and cold-end temperatures (T_{H} and T_{L}), respectively. Meanwhile, a nickel chromium heating wire powered by a direct current source is wound around the cold-end heat exchanger to measure the cooling power. The measured parameters, related instruments, and measurement uncertainties are listed in Table 1.

Table 1. Uncertainties of the experimental measurements.

Parameters	Instruments	Range	Uncertainties
Thermal diffusivity ($mm^2 \cdot s^{-1}$)	NETZSCH LFA 427	0.1–1000	2.2%
Density ($kg \cdot m^{-3}$)	Sartorius ENTRIS64-1S	0.0001–60	0.1 %
Specific heat ($J \cdot kg^{-1} \cdot K^{-1}$)	PPMS	1.9–400	2%
Temperature (K)	PT100 thermometer	80–400	±0.1 K
Cooling power (W)	LW DC power supply	0–192	2.4%

3.2. Property measurement results

Figure 3 shows the SEM images of pure LFCSC particles (see Fig. 3(a)) and the fracture surfaces of LFCSC/PR compounds. Besides LFCSC particles, the other phase that strongly adheres to the partial surface of the alloy particles and bonds the particles together with a flexible morphology is the cured phenolic resin (see Figs. 3(b) and 3(c)). The bright white areas are attributed to the phenolic resin. These can be further confirmed by EDS analysis at several areas marked as *a*–*e* in the SEM images (presented in Table 2). It can be seen that compositions and element proportions of the surfaces of alloy particles in these compounds are almost in line with that of pure LFCSC, while flexible phases b and e display a great quantity of C atoms, O atoms, and a negligible amount of La, Fe, Co, Si. As shown in Fig. 3(b), alloy particles, whether big or small, are in close contact with each other. Small particles occupy voids between adjacent big particles. Only partial surfaces of the alloy particles are coated by the cured phenolic resin. It is noted that the resin strongly bonds contiguous particles together and does not break the contacts between particles, which ensures the mechanical strength of the compound and smooth heat transfer channels. This special structure of the 97.5-LFCSC compound arises from using solid binder of phenolic resin powders rather than liquid polymer. One could imagine that if liquid polymer is used, it would fully cover the surface of all alloy particles, even block those direct contact sites between alloy particles. As the mass fraction of the phenolic resin increases to 5 wt%, the architectural features of the LFCSC/PR compounds still remained, except that there are more resin covering on the partial surfaces of alloy particles and filling the voids between particles without breaking their contact (shown in Fig. 3(c)).

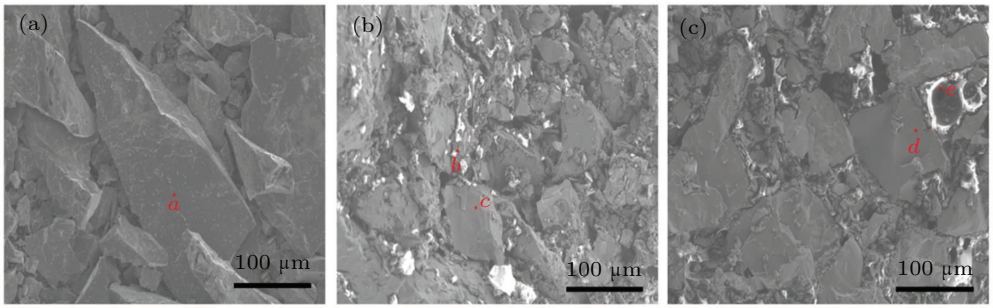


Fig. 3. SEM images of (a) pure LFCSC particles, (b) the fracture surface of 97.5-LFCSC, and (c) the fracture surface of 95-LFCSC.

Table 2. EDS analysis of areas marked as a∼e in the SEM images.

Atomic (%)	La	Fe	Co	Si	C	O
$LaFe_{10.87}Co_{0.63}Si_{1.5}C_{0.2}$	7.04	76.55	4.44	10.56	1.41	0
a	7.79	79.01	5.00	6.47	1.73	0
b	2.02	13.93	0.71	0.60	70.11	12.62
c	7.51	73.33	4.25	10.81	4.10	0
d	7.62	75.23	4.65	10.13	2.37	0
e	3.08	6.18	0	0.34	62.06	28.34

Figure 4(a) shows powder XRD patterns of pure LFCSC alloy and LFCSC/PR compounds. For pure LFCSC alloy, all the diffraction peaks belong to cubic $NaZn_{13}$-type structure (1:13 phase), and there is no apparent secondary phase, such as α-Fe phase or La-rich phase. In the case of 97.5-LFCSC and 95-LFCSC compounds, the diffraction peak positions remain exactly the same with that of pure LFCSC, which suggests that the $NaZn_{13}$-type structures remain unchanged when covering with the cured PR. Furthermore, there are no obvious impurity phases as well.

Temperature dependence of magnetic entropy change ΔS for pristine LFCSC alloy and its compounds are shown in Fig. 4(b). The maximum value of $|\Delta S|$ for the pristine LFCSC alloy was 5.30 $J{\cdot}kg^{-1}{\cdot}K^{-1}$ ($\mu\Delta H = 2$ T), which was attributed to the field-induced IEM from the PM to FM and the concurrent negative lattice expansion above the T_c. Magnetic entropy change ΔS for the 97.5-LFCSC and 95-LFCSC are nearly the same with that of pristine alloy, which is not surprising since non-magnetic PR would not disturb the magnetic field generated by the permanent magnet and not destroy the crystal structures of magnetic materials. Due to the dilution effect caused by the addition of polymer and the sampling errors, the ΔS values of these compounds are somewhat lower than that of pure magnetic materials. The maximum magnetic entropy ΔS_m are 5.06 $J{\cdot}kg^{-1}{\cdot}K^{-1}$ for 97.5-LFCSC compound and 4.99 $J{\cdot}kg^{-1}{\cdot}K^{-1}$ for 95-LFCSC compound, which decreased by 4.5% and 5.8%, respectively, compared with that of pristine LFCSC alloys.

To obtain a high performance AMR, excellent thermal transport properties are very crucial. Table 3 shows the thermal conductivity κ of LFCSC, 97.5-LFCSC, and 95-LFCSC at 304 K (Each compound has two samples being tested). The thermal conductivity of LFCSC is 8.67 $W{\cdot}m^{-1}{\cdot}K^{-1}$, and the thermal conductivity is reduced to 3.01 $W{\cdot}m^{-1}{\cdot}K^{-1}$ for 97.5-LFCSC. This is due to the porous structure of bonded 97.5-LFCSC composites. Although LFCSC particles may contact each other, there is very large thermal contact resistance, coupled with low thermal conductivity of the resin filled in the pores between the particles, resulting in a decrease in the thermal conductivity of composite materi-

als. But the thermal conductivity of 97.5-LFCSC is apparently higher than that of the reported porous $LaFe_{11.6}Si_{1.4}H_y$ (2.0 $W{\cdot}m^{-1}{\cdot}K^{-1}$ at 300 K)[34] and $LaFe_{11.6}Si_{1.4}$/3.0-wt% Cu compounds (2.7 $W{\cdot}m^{-1}{\cdot}K^{-1}$ at 300 K, Cu plating before cold pressing)[36] with particle sizes of raw materials ranging from 177 μm to 250 μm. The relatively high values of these two samples are due to the reason that the point contacts between adjacent alloy particles provide good conductive paths, which is in coincidence with the SEM analysis (shown in Fig. 4). As the mass fraction of Phenolic Resins (PR) increased from 2.5 to 5.0, the thermal conductivity of this composite material was increased to 3.13 $W{\cdot}m^{-1}{\cdot}K^{-1}$, which further proved that the increased PR filled the pores between the magnetic particles without destroying the magnetic properties contact between particles. The thermal conductivities of 95-LFCSC and 97.5-LFCSC are higher than that of $La_{1-x}Ca_xMnO_3$ (1 $W{\cdot}m^{-1}{\cdot}K^{-1}$–2 $W{\cdot}m^{-1}{\cdot}K^{-1}$)[37] and MnAs ($\sim$ 2 $W{\cdot}m^{-1}{\cdot}K^{-1}$)[38] magnetocaloric materials, which is beneficial to attaining a relatively high cooling power.[27] The following experiments are all based on 95-LFCSC.

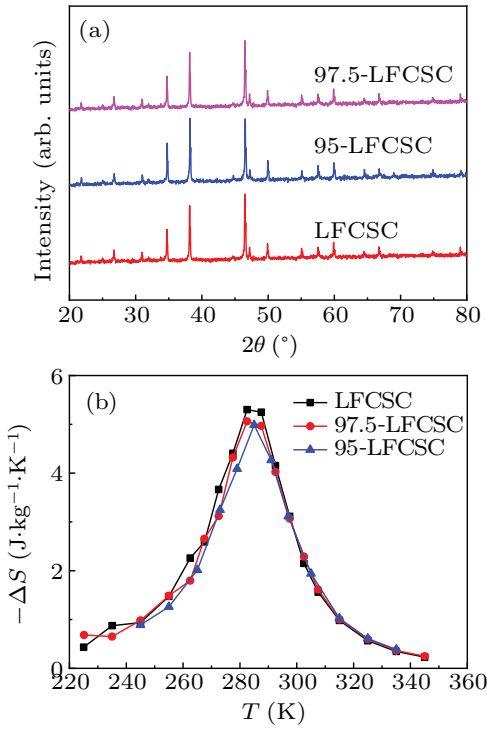


Fig. 4. (a) The x-ray diffraction patterns of the pure LFCSC alloy, 97.5-LFCSC, and 95-LFCSC. (b) Entropy change ΔS as a function of temperature under a field change of 0 T–2 T for LFCSC, 97.5-LFCSC, and 95-LFCSC.

Table 3. The thermal conductivity κ of LFCSC, 97.5-LFCSC, and 95-LFCSC at 304 K.

Material	κ ($W{\cdot}m^{-1}{\cdot}K^{-1}$)		
	First sample	Second sample	Average
LFCSC	8.68	8.65	8.67
97.5-LFCSC	3.12	2.89	3.01
95-LFCSC	3.23	3.03	3.13

The isothermal magnetic entropy changes $-\Delta S_M$ of $La(Fe_{11.6-x}Co_x)Si_{1.4}C_{0.15}$ (x = 0.6, 0.65, 0.7, 0.75, 0.8, 0.85)/PR compounds with 5-wt% PR are obtained from the experimental isothermal magnetization data by using the Maxwell relation

$$\Delta S(T,H) = \int_0^H (\partial M/\partial T)_H \, \mathrm{d}H.$$

Figure 5 shows the temperature dependences of $-\Delta S_M$ for magnetic field changes 2 T. The maximum values of magnetic entropy change ($-\Delta S_M^{max}$) are 7.1, 7.0, 4.8, 5.9, 6.0, and 5.3 $J{\cdot}kg^{-1}{\cdot}K^{-1}$, respectively. The $-\Delta S_M^{max}$ decreased monotonically for $La(Fe_{11.6-x}Co_x)Si_{1.4}C_{0.15}$/PR compounds with decreased x except at x = 0.7. The reason for this may be the error that was made in the processing of $La(Fe_{11.6-x}Co_x)Si_{1.4}C_{0.15}$ (x = 0.7). For this reason, this compound was not used in the next experiments.

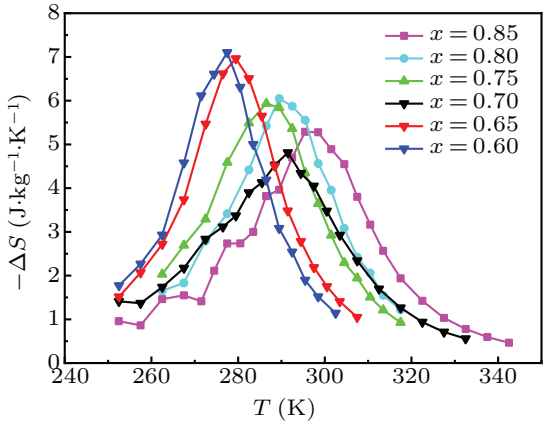


Fig. 5. The magnetic entropy change as a function of temperature for the $La(Fe_{11.6-x}Co_x)Si_{1.4}C_{0.15}$ (x = 0.6, 0.65, 0.7, 0.75, 0.8, 0.85)/PR compounds under 0 T–2 T.

The volumetric entropy change is more important from the practical point of view.[1] For a magnetic refrigerator, the designer needs to know the cooling per unit volume, and thus it is more meaningful to use volumetric ΔS_m to evaluate the usage of magnetocaloric materials. Through density measurements, which was measured by the Archimedean method, the calculated results of the maximum $La(Fe_{11.6-x}Co_x)Si_{1.4}C_{0.15}$ (x =0.6, 0.65, 0.75, 0.8, 0.85)/PR volumetric magnetic entropy are 36.4, 35.9, 30.4, 3.9, and 27.4 $mJ{\cdot}cm^3{\cdot}K^{-1}$, respectively. As compared with the value of pure $La(Fe_{11.6-x}Co_x)Si_{1.4}C_{0.15}$, which are about 49.6, 48.4, 41.6, 43.0, 37.6 $mJ{\cdot}cm^3{\cdot}K^{-1}$, respectively, the volumetric magnetic entropy decrease 26.7%, 25.5%, 26.9%, 28.1%, 27.1%, respectively. The reduction of the volumetric ΔS_m mostly result from the porous structure of the composite material and the presence of low density resin.

As shown in Fig. 5, the changing Curie temperature with x content within the temperature range roughly from 27 K to 300 K is very useful for refrigerator working around this temperature span.

4. Regenerator construction and its test in hybrid magnetic refrigerator

In order to evaluate the cooling performance of the La(Fe,Si)$_{13}$-based/PR plates in a magnetic refrigerator, a multi-layered La(Fe$_{11.6-x}$Co$_x$)Si$_{1.4}$C$_{0.15}$ ($x = 0.60$, 0.65, 0.75, 0.80, 0.85)/PR (with 5-wt% PR) AMR has been constructed. The disc-shaped samples with a thickness of 0.5 mm were cut into plates (10-mm wide). These plates were filled in stainless steel rings (inner diameter of 44.5 mm, thickness of 0.5 mm) in series to form parallel plate regenerators with a plate spacing of 0.5 mm (shown in Fig. 6). A hybrid refrigerator combining the active magnetic refrigeration effect and the Stirling cycle refrigeration effect[39] has been used to test the multi-layered AMR which is made up of 8 sections of parallel plate regenerators (two $x = 0.65$ sections, two $x = 0.8$ sections). Figure 7 illustrates the system configuration. The main components of the hybrid refrigerator include: a compression piston with cylinder, an expansion piston with cylinder, a hot heat exchanger (HHEX), a regenerator, a cold-end heat exchanger (CHEX), a thermal buffer tube, and a magnet. Among them, the HHEX, the regenerator and the CHEX are shared by both the Stirling cycle refrigerator, and the magnetic refrigerator. The regenerator is held stationary within the magnetic field.

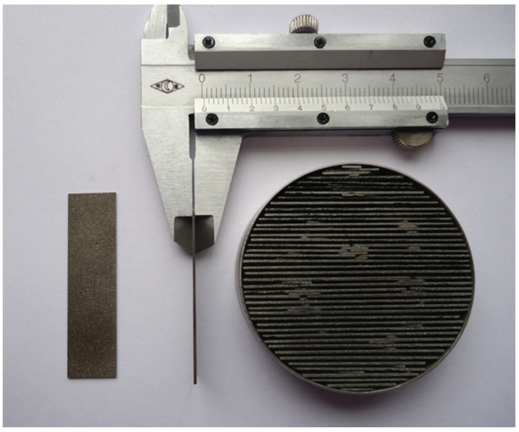


Fig. 6. Photograph of La(Fe$_{11.6-x}$Co$_x$)Si$_{1.4}$C$_{0.15}$/PR plates with a thickness of 0.5 mm and a layer cross-section view of regenerator made out of these parallel plates.

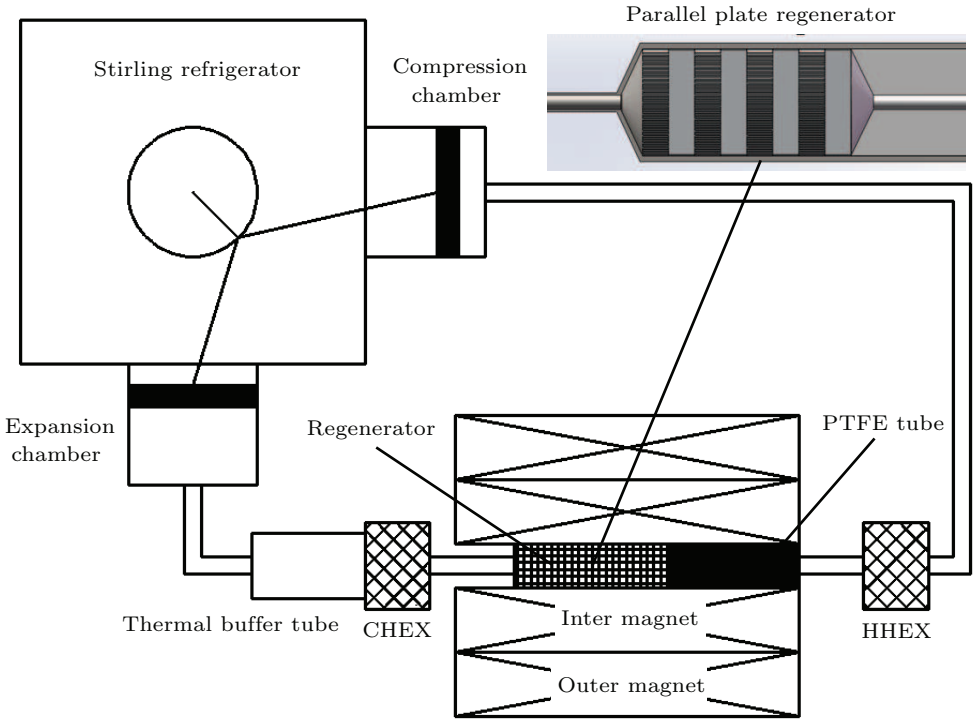


Fig. 7. Schematic diagram of the hybrid refrigerator.

Figure 8 shows that the measured cooling power of the system as a function of time at a charged helium pressure of 4.5 MPa and operating frequency of 2.5 Hz, where cooling curves with and without the MCE are illustrated. With and without the MCE are the hybrid mode and the pure Stirling cycle mode, respectively. The temperature span is defined to be hot-end temperature T_H minus cold-end temperature T_L and the simulated cooling load in the system is provided by a nickel–chromium heating wire and a DC power supply. Figure 8 clearly shows that the cooling performance of the hybrid machine at $\alpha = 60^\circ$ is better than that of pure Stirling cycle refrigeration at the same operation conditions. The phase angle is defined as phase difference between the maximum value of varying compression volume and the maximum value of varying magnetic field. The phase angle represents the relationship between the applied magnet field and heat transfer fluid flow rate. At the phase angle of 60°, hybrid refrigerator achieved maximum efficiency. The system has produced a maximum

no-load temperature span of 41 K and cooling power of 41 W over a temperature span of 30 K. With the same operation conditions, the temperature spans and cooling power in the hybrid machine have increased compared to pure Stirling cycle refrigeration.

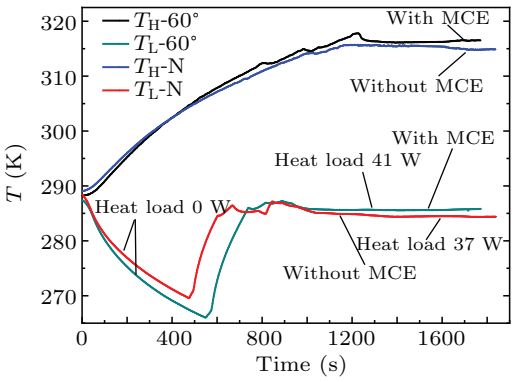


Fig. 8. The cooling-down curves for using the multi-layer $La(Fe_{11.6-x}Co_x)Si_{1.4}C_{0.15}$ (x = 0.60, 0.65, 0.75, 0.80, and 0.85)/PR AMR at 4.5 MPa and 2.5 Hz.

The result is worse than that obtained from the previous study using Gd.[39] The reason for this mostly is that the thermal conductivity of Gd plates (10.6 $W{\cdot}m^{-1}{\cdot}K^{-1}$) is better than the phenolic resin bonded $La(Fe,Si)_{13}$-based plates. The ability of transfer heat from the magnetic material to the heat transfer fluid is one of the most important determining factors of the AMR efficiency. On the other hand, in AMR designs heat transfer within the magnetic material along the bed in the direction of the fluid flow would diminish the efficiency of the AMR. Therefore, it depends on not only the large MCE of the refrigerant material but also the excellent thermal transport properties. The performance of a magnetic refrigerator even need to design the thermal conductivity of the magnetic material to achieve an anisotropic distribution of the thermal conductivity. That is a lower thermal conductivity of the magnetocaloric material in the streamwise direction would lead to higher performances in the regenerator. Thus, the regenerator bed including eight separated parallel plate regenerators have been designed (shown in Fig. 7), in order to improve the thermal resistance along the length of a parallel-plate magnetic regenerator.

5. Conclusion

This paper presents a simple procedure which was developed for processing brittle $La(Fe,Si)_{13}$ towards high performance magnetic refrigerants. It is a promising molding process for producing mechanically stable refrigerants with excellent magnetic cooling effect. A compound of $La(Fe,Si)_{13}$-based alloy powders and thermoset phenolic resin powders was hot pressed at 150 °C and 20 MPa to obtain plate-shaped $La(Fe,Si)_{13}$/PR compound magnetic refrigerants. Through incorporation of 2.5-wt% PR and 5-wt% PR, the maximum entropy change ΔS_m per unit mass of LFCSC was decreased by 4.5% and 5.8%, respectively. That is, the large entropy change ΔS remained. It is particularly worth mentioning that the thermal conductivity of the LFCSC/PR compound with 5-wt% PR could reach up to 3.13 $W{\cdot}m^{-1}{\cdot}K^{-1}$. The $La(Fe_{11.6-x}Co_x)Si_{1.4}C_{0.15}$ (x = 0.60, 0.65, 0.75, 0.80, 0.85)/phenolic resin compounds were pressed into thin plates and tested in a hybrid refrigerator that combines the active magnetic refrigeration effect with the Stirling cycle refrigeration effect. Testing using multilayer $La(Fe_{11.6-x}Co_x)Si_{1.4}C_{0.15}$ (x = 0.60, 0.65, 0.75, 0.80, 0.85)/PR AMR gives a maximum cooling power of 41 W over a temperature span of 30 K under a pressure of 4.5 MPa and a frequency of 2.5 Hz.

Unlike those processes that use additional chemistry reagents, high temperature, high pressure or complex equipment, this work represents an environmentally friendly and energy-efficient process for manufacturing regularly-shaped magnetic refrigerants. The excellent magnetocaloric effect and reasonable thermal conductivities of the $La(Fe,Si)_{13}$/PR compound magnetic refrigerant, in addition to the very low material costs, easy fabrication, and molding, make it an attractive candidate for commercial magnetic refrigerator.

Moreover, this method is also suitable for fabricating plate-shaped $La(Fe,Si)_{13}H_\delta$/PR compounds given a well-controlled heating temperature.

Acknowledgements

Project supported by the National Natural Science Foundation of China (Grant Nos. 52171054 and 52171195) and the National Natural Science Foundation for Distinguished Young Scholars (Grant No. 51925605).

References

[1] Benke D, Fries M, Specht M, Wortmann J, Pabst M, Gottschall T, Radulov I, Skokov K, Bevan AI, Prosperi D, Tudor C O, Afiuny P, Zakotnik M and Gutfleisc O 2020 *Energy Technol.* **8** 1901025
[2] Kitanovski A 2020 *Adv. Energy Mater.* **10** 1903741
[3] Tang X, Sepehri-Amin H, Terada N, Martin-Cid A, Kurniawan I, Kobayashi S, Kotani Y, Takeya H, Lai J, Matsushita Y, Ohkubo T, Miura Y, Nakamura T and Hono K 2022 *Nat. Commun.* **13** 1817
[4] Smith A, Bahl C R H, Bjørk R, Engelbrecht K, Nielsen K K and Pryds N 2012 *Adv. Energy Mater.* **2** 1288
[5] Pecharsky V K and Gschneidner K A Jr 1999 *J. Magn. Magn. Mater.* **200** 44
[6] Rowe A M and Barclay J A 2003 *J. Appl. Phys.* **93** 1672
[7] Pecharsky V K and Gschneidner K A Jr 1997 *Phys. Rev. Lett.* **78** 4494
[8] Pecharsky V K and Gschneidner K A Jr 1997 *Appl. Phys. Lett.* **70** 3299
[9] Provenzano V, Shapiro A J and Shull R D 2004 *Nature* **429** 853
[10] Zhou H, Long Y, Miraglia S, Porcher F and Zhang H 2022 *Rare Metals* **41** 992
[11] Zhang H, Sun Y J, Li Y W, Wu Y Y, Long Y, Shen J, Hu F X, Sun J R and Shen B G 2015 *J. Appl. Phys.* **117** 063902
[12] Campos A D, Rocco D L, Carvalho A M G, Caron L, Coelho A A, Gama S, Silva L M D, Gandra F C G, Santos A O D, Cardoso L P, Ranke P J V and Oliveira N A D 2006 *Nat. Mater.* **5** 802

[13] Tegus O, Brück E, Buschow K H J and Boer F R D 2002 *Nature* **415** 150

[14] Aliev A M, Khanov L N, Gamzatov A G, Batdalov A B, Kurbanova D R, Yanushkevich K I and Govor G A 2021 *Appl. Phys. Lett.* **118** 072404

[15] Cong D Y, Huang L, Hardy V, Bourgault D, Sun X M, Nie Z H, Wang M G, Ren Y, Entel P and Wang Y D 2018 *Acta Mater.* **146** 142

[16] Krenke T, Duman E, Acet M, Wassermann E F, Moya X, Manosa L and Planes A 2005 *Nat. Mater.* **4** 450

[17] Liu J, Gottschall T, Skokov K P, Moore J D and Gutfleisch O 2012 *Nat. Mater.* **11** 620

[18] Eerenstein W, Wiora M, Prieto J L, Scott J F and Mathur N D 2007 *Nat. Mater.* **6** 348

[19] Moya X, Hueso L E, Maccherozzi F, Tovstolytkin A I, Podyalovskii D I, Ducati C, Phillips L C, Ghidini M, Hovorka O, Berger A, Vickers M E, Defay E, Dhesi S S and Mathur N D 2013 *Nat. Mater.* **12** 52

[20] Zhang X X, Tejada J, Xin Y, Sun G F, Wong K W and Bohigas X 1996 *Appl. Phys. Lett.* **69** 3596

[21] Kavita S, Alagusoundarya M, Ramakrishna V V, Suresh V, Pramod Bhatt, Srimathif P, Archanaa R, Debendranath Kar, Tiju Thomas and Gopalana R 2022 *J. Alloys Compd.* **895** 162597

[22] Krautz M, Skokov K, Gottschall T, Teixeirac C S, Waske A, Liu J, Schultz L and Gutfleisch O 2014 *J. Alloys Compd.* **598** 27

[23] Franco V, Law J Y, Conde A, Brabander V, Karpenkov D Y, Radulov I, Skokov K and Gutfleisch O 2017 *J. Phys. D: Appl. Phys.* **50** 414004

[24] Zhang H, Hu F X, Sun J R and Shen B G 2013 *Sci. China-Phys. Mech. Astron.* **56** 2302

[25] Zhang M K, Abdelaziz O, Momen M A and Abu-Heiba A 2017 *Sci. Rep.* **7** 13962

[26] Paul-Boncour V and Bessais L 2021 *Magnetochemistry* **7** 13

[27] Nielsen K K and Engelbrecht K 2012 *J. Phys. D: Appl. Phys.* **45** 145001

[28] Yu B F, Liu M, Egolf P W and Kitanovski A 2010 *Int. J. Refrig.* **33** 1029

[29] Fujita A, Koiwai S, Fujieda S, Fukamichi K, Kobayashi T, Tsuji H, Kaji S and Saito A T 2009 *J. Appl. Phys.* **105** 07A936

[30] Saito A T, Kobayashi T and Tsuji H 2007 *J. Magn. Magn. Mater.* **310** 2808

[31] Katter M, Zellmann V and Barcza A 2010 4*th Int. Conference on Magnetic Refrigeration at Room Temperature*, Baotou, China, August 23–28, 2010 p. 49

[32] Moore J D, Klemm D, Lindackers D, Grasemann S, Trager R, Eckert J, Lober L, Scudino S, Katter M, Barcza A, Skokov K P and Gutfleisch O 2013 *J. Appl. Phys.* **114** 043907

[33] Tian N, Zhang N N, You C Y, Gao B and He J 2013 *J. Appl. Phys.* **113** 103909

[34] Lyubina J, Schafer R, Martin N, Schultz L and Gutfleisch O 2010 *Adv. Mater.* **22** 3735

[35] Shao Y Y, Liu J, Zhang M X, Aru Yan, Konstantin P.Skokov, Dmitriy Yu Karpenkov and Oliver Gutfleisch 2017 *Acta Mater.* **125** 506

[36] Lyubina J, Hannemann U, Cohen L F and Ryan M P 2012 *Adv. Energy Mater.* **2** 1323

[37] Cohn J L, Neumeier J J, Popoviciu C P, McClellan K J and Leventouri T 1997 *Phys. Rev. B* **56** R8495

[38] Fujieda S, Hasegawa Y, Fujita A and Fukamichi K 2004 *J. Appl. Phys.* **95** 2429

[39] Gao X Q, Shen J, He X N, Tang C C, Li K, Dai W, Li Z X, Jia J C, Gong M Q and Wu J F 2016 *Int. J. Refrigeration* **67** 330